Published in final edited form as:
Biochemistry. 2008 February 5; 47(5): 1326–1335. doi:10.1021/bi701594j.

Functional Role of Residue 193 (Chymotrypsin Numbering) in Serine Proteases: Influence of Side Chain Length and β-Branching on the Catalytic Activity of Blood Coagulation Factor XIa†

Amy E. Schmidt‡, **Mao-fu Sun**§, **Taketoshi Ogawa**§, **S. Paul Bajaj***,‡, and **David Gailani***,§
UCLA/Orthopaedic Hospital, Department of Orthopaedic Surgery and Molecular Biology Institute, David Geffen School of Medicine at UCLA, Los Angeles, California 90095, and the Departments of Pathology and Medicine, Vanderbilt University, Nashville, Tennessee 37232

Abstract

In serine proteases, Gly^{193} (chymotrypsin numbering) is conserved with rare exception. Mutants of blood coagulation proteases have been reported with Glu, Ala, Arg or Val substitutions for Gly^{193}. To further understand the role of Gly^{193} in protease activity, we replaced it with Ala or Val in coagulation factor XIa (FXIa). For comparison to the reported FXIa Glu^{193} mutant, we prepared FXIa with Asp (short side chain) or Lys (opposite charge) substitutions. Binding of *p*-aminobenzamidine (*p*AB) and diisopropylfluorphosphate (DFP) were impaired 1.6–36-fold and 35–478-fold, respectively, indicating distortion of, or altered accessibility to, the S1 and oxyanion-binding sites. Val or Asp substitutions caused the most impairment. Salt bridge formation between the amino terminus of the mature protease moiety at Ile^{16} and Asp^{194}, essential for catalysis, was impaired 1.4–4-fold. Mutations reduced catalytic efficiency of tripeptide substrate hydrolysis 6–280-fold, with Val or Asp causing the most impairment. Further studies were directed toward macromolecular interactions with the FXIa mutants. k_{cat} for factor IX activation was reduced 8-fold for Ala and 400–1100-fold for other mutants, while binding of the inhibitors antithrombin and amyloid β-precursor protein Kunitz domain (APPI) was impaired 13–2300-fold and 22–27000-fold, respectively. The data indicate that β-branching of the side chain of residue 193 is deleterious for interactions with *p*AB, DFP and amidolytic substrates, situations where no S2′–P2′ interactions are involved. When an S2′–P2′ interaction is involved (factor IX, antithrombin, APPI), β-branching and increased side chain length are detrimental. Molecular models indicate that the mutants have impaired S2′ binding sites and that β-branching causes steric conflicts with the FXIa 140-loop, which could perturb the local tertiary structure of the protease domain. In conclusion, enzyme activity is impaired in FXIa when Gly^{193} is replaced by a non-Gly residue, and residues with side chains that branch at the β-carbon have the greatest effect on catalysis and binding of substrates.

Serine proteases play an essential role in many biologic processes including digestion of dietary proteins, blood coagulation, the complement cascades, fibrinolysis, bone resorption and remodeling, cell differentiation, and fertilization (1-7). The cleft shaped active site of the

†This work was supported by Awards HL36365 and HL70369 to S.P.B. and HL58837 to D.G. from the National Heart, Lung, and Blood Institute.

*Correspondence. D.G.: Hematology/Oncology Division, Vanderbilt University, 777 Preston Research Building, 2220 Pierce Ave., Nashville, TN 37232-6307; tel, (615) 936-1505; fax, (615) 936-3853; dave.gailani@vanderbilt.edu. S.P.B.: Protein Science Laboratory, UCLA/Orthopaedic Hospital, Department of Orthopaedic Surgery and Molecular Biology Institute, Box 951795, Los Angeles, CA 90095-1795; tel, (310) 825-5622; fax, (310) 825-5972; pbajaj@ mednet.ucla.edu. .
‡David Geffen School of Medicine at UCLA.
§Vanderbilt University.

chymotrypsin/trypsin family of serine proteases contains a catalytic triad comprising residues His^{57}, Asp^{102}, and Ser^{195} (chymotrypsin numbering system)[1] (8). These residues are located at the entrance to the substrate-binding pocket, where the $N\epsilon_2$ of His^{57} is poised to accept a proton from the $O\gamma$ of Ser^{195} during the nucleophilic attack by this oxygen on the carbonyl carbon of the substrate. The negatively charged carboxyl group of Asp^{102} serves to stabilize the positively charged form of His^{57} by making an H-bond with $N\epsilon_1$ of His^{57}. This charge relay system makes Ser^{195}-$O\gamma$ an unusually strong nucleophile and permits peptide bond hydrolysis (9).

Amino acids from the amino terminus to carboxy terminus of the substrate are designated P*n*, …, P3, P2, P1, P1′, P2′, P3′, …, P*n*', with peptide bond cleavage occurring between residues P1 and P1′. The corresponding binding sites on the enzyme are designated S*n*, …, S3, S2, S1, S1′, S2′, S3′, …, S*n*' (10). In trypsin-like proteases, Asp^{189} is at the bottom of the S1 site, and forms a salt bridge with the guanidinium or the ammonium group of the P1 Arg or Lys, respectively, of the substrate (9). Another defining feature of serine proteases, including those containing divergent folds from chymotrypsin, subtilisin, and serine carboxypeptidase families, is the presence of an oxyanion-binding site (9). In the chymotrypsin/trypsin family, the oxyanion binding site is formed by the backbone amide nitrogens of Gly^{193} and Ser^{195}. The nucleophilic attack by the $O\gamma$ of Ser^{195} on the carbonyl carbon atom of the substrate changes the geometry around this carbon from trigonal planar to tetrahedral. The tetrahedral reaction intermediate is intrinsically unstable due to the negative charge on the peptide carbonyl oxygen atom. However, in serine proteases this charged oxyanion is stabilized by hydrogen bonds with the amide NH groups of Gly^{193} and Ser^{195} in a location referred to as the oxyanion hole. These interactions result in preferential binding of the substrate in the transition state, a necessary requirement for enzyme catalysis.

Gly^{193} is conserved in nearly all serine proteases (9-13) and is part of a type II β-turn. In the FXIa[2] structure, the φ-ψ conformation parameters for residue 193 are similar to those in many serine protease crystal structures [RCSB Protein Data Bank], and are in a region of the Ramachandran plot that is compatible only with a Gly residue. The β-carbon of a non-Gly residue would have a steric conflict with the carbonyl O of residue 192, resulting in a type I β-turn that causes the amide nitrogen of residue 193 to point away from the oxyanion hole, disrupting the oxyanion binding site and the S1 site (14). In addition, the side chain of a non-Gly 193 residue is expected to occupy the S2′ site, interfering with S2′–P2′ interactions. Therefore, the side chain length, charge, and conformation at residue 193 are expected to play a significant role in determining the extent of dysfunction for a mutant protein.

Naturally occurring mutations at position 193 have been identified in plasma coagulation proteases, including Gly → Glu[1] in factor XI (FXI)[>2], Gly → Ala, Arg, Val or Glu in factor IX (FIX), and Gly → Glu or Arg in factor VII (FVII) (15-22). FXIa, the active form of the homodimeric protease zymogen FXI (23), is a component of a pathway involved in sustaining thrombin generation at a wound site (24). FXIa has considerably higher amidolytic activity toward tripeptide chromogenic substrates when compared to FVIIa and FIXa, and FXIa interactions with macromolecular substrates and inhibitors are reasonably well-defined. For these reasons, we chose FXIa as a model coagulation enzyme to study the effects of amino acid substitutions for Gly^{193}. The data indicate that β-branching and side chain length play a significant role in determining the degree of enzyme impairment.

[1]The chymotrypsin amino acid numbering system is used to assign numbers to amino acids in the FXIa catalytic domain, and is used throughout the manuscript. Gly^{193} in chymotrypsin corresponds to Gly^{555} in FXIa, Gly^{363} in factor IXa and Gly^{342} in factor VIIa. Chymotrypsin Ile^{16} and Asp^{194} correspond to FXIa Ile^{370} and Asp^{556}, respectively.

EXPERIMENTAL PROCEDURES

Reagents and Proteins

H-D-Ile-Pro-Arg-*p*-nitroanilide (S-2288) and pyroGlu-Pro-Arg-*p*-nitroanilide (S-2366), were from DiaPharma (West Chester, OH). Sodium boro[^{3}H]-hydride was from Perkin-Elmer. Enhanced chemiluminescence (ECL) detection reagents were from Amersham Pharmacia Biotech. Diisopropylfluorophosphate (DFP) was from Calbiochem. Activated partial thromboplastin reagent was from Beckman Coulter, and normal plasma was from George King (Overland Park, KS). Unfractionated heparin was from Pharmacia Hepar, Inc. (Franklin, OH). Fatty acid free bovine serum albumin (BSA), *p*-aminobenzamidine (*p*AB), polyethylene glycol 8000 (PEG), Polybrene, and other chemicals of the highest grade available were from Sigma. Corn trypsin inhibitor (CTI), human FXIIa, FIX, and antithrombin were from Enzyme Research Laboratories (South Bend, IN). The Kunitz domain of protease Nexin-2/ amyloid β Protein Precursor Kunitz protein inhibitor (APPI) was a gift from Dr. Alvin Schmaier (Case-Western Reserve University, Cleveland).

Expression and Purification of Recombinant FXI Proteins

The GGA triplet coding for Gly^{555} (corresponds to chymotrypsin Gly^{193}) in the FXI cDNA (nucleotides 1760–1762) (25) was changed to GCA (Ala), GTA (Val), GAA (Glu), GAC (Asp), or AAA (Lys) using a QuikChange mutagenesis kit (Stratagene). The cDNAs were ligated into mammalian expression vector pJVCMV, which contains a cytomegalovirus promoter, as described (26). 293 fetal kidney fibroblasts (5×10^6, ATCC CRL 1573) were transfected by electroporation (Electrocell Manipulator 600 BTX, San Diego) with 40 μg of pJVCMV-FXI construct and 2 μg of pRSVneo that contains a cDNA conferring neomycin resistance. Cells

[2]Abbreviations:

FXI	factor XI
FXI$_a$	factor XIa
FIX	factor IX
FVII	factor VII
***p*AB**	*p*-aminobenzamidine
CTI	corn trypsin inhibitor
APPI	amyloid β protein precursor Kunitz domain inhibitor
TCA	trichloracetic acid
TBS	50 mM Tris-HCl, 150 mM NaCl, pH 7.5
***p*NA**	*p*-nitroaniline
S-2288	H-D-Ile-Pro-Arg-*p*-nitroanilide
S-2366	pyroGlu-Pro-Arg-*p*-nitroanilide
BSA	bovine serum albumin
PEG	polyethylene glycol 8000
HBSP	20 mM Hepes, 0.15 M NaCl, 0.1% PEG, 2 mM $CaCl_2$, pH 7.5
Tris/NaCl/T	25 mM Tris-HCl, 100 mM NaCl pH 7.4, plus 0.1% Tween-20
DFP	diisopropylfluorophosphate
BPTI	bovine pancreatic trypsin inhibitor

were grown in DMEM with 5% fetal bovine serum and 500 μg/mL G418, and supernatants from G418 resistant clones were tested for protein expression by ELISA using goat anti-human FXI polyclonal antibodies (Affinity Biologicals, Hamilton, Ontario). Expressing clones were expanded in 175 cm^2 flasks using Cellgro Complete media (Mediatech, Herndon, VA). Conditioned medium was collected every 48–72 h, supplemented with benzamidine (5 mM), and stored at −20 °C.

Proteins were purified by monoclonal antibody affinity chromatography from 1 L of conditioned medium using an anti-FXI IgG 1G5.12 monoclonal affinity column (26), and stored in Tris-HCl 50 mM pH 7.5, 150 mM NaCl (TBS). Protein concentration was determined by dye binding assay (BioRad, Hercules, CA), and purity by SDS–PAGE. Purified proteins were homogeneous on SDS–PAGE with the correct molecular mass for a FXI homodimer. To prepare FXIa, FXI (300 μg/mL) was incubated with 5 μg/mL FXIIa at 37 °C, and complete conversion to FXIa was confirmed by reducing SDS-PAGE. FXIIa was inhibited with 20-fold molar excess of CTI. Wild type FXIa is designated hereafter as $FXIa_{WT}$, while mutant FXIa is designated $FXIa_{G193A}$, $FXIa_{G193V}$, $FXIa_{G193E}$, $FXIa_{G193D}$, or $FXIa_{G193K}$.

Measurement of FXIa Amidolytic Activity

Each reaction contained TBS with 5 mM Ca^{2+}, 100 μg/mL BSA, 0.5 nM $FXIa_{WT}$ or 2–5 nM $FXIa_{G193}$ mutant proteins, and different amounts of S-2288 or S-2366. The rate of *p*NA release was measured using a Beckman DU800 spectrophotometer with kinetics module at 405 nm for 15 min. The amount of *p*NA released was calculated using an extinction coefficient of 9.9 mM^{-1}, cm^{-1} at 405 nM (27). The initial rate was converted to μM substrate hydrolyzed/min. The program GraFit was used to determine K_m and V_{max}, using the Enzyme Kinetics Program from Erithacus Software.

Inhibition of FXIa by DFP

Each reaction mixture contained 250 nM FXIa in TBS with 100 μg/mL BSA and 5 mM $CaCl_2$. Increasing amounts of DFP (2 μM to 0.8 mM) were added to each reaction and incubated at room temperature. At various time points, 5 μL aliquots were removed and added to 155 μL of TBS with 100 μg/mL BSA containing 625 μM S-2288. Changes in absorbance at 405 nm were measured, and residual FXIa activity was determined at each time point. Residual activity was plotted as a percent of initial activity, and the first-order rate constants (k_{obs}) for each concentration of DFP were obtained using eq 1,

$$A_t = A_0 \exp(-k_{obs} t) \quad (1)$$

where A_t and A_0 are the percent FXIa activity at time t and 0 s, respectively. Values for k_{obs} were plotted against DFP concentration to obtain second-order rate constants.

Determination of $K_{d(app)}$ for Binding of pAB to FXIa

The $K_{d(app)}$ was determined by analyzing competitive inhibition of S-2288 hydrolysis. Reactions were carried out in TBS with 100 μg/mL BSA and 5 mM $CaCl_2$ and either 100 μM S-2288 (for $FXIa_{WT}$) or 500 μM S-2288 (for $FXIa_{G193}$ mutants). Increasing amounts of *p*AB were added, and reactions were initiated by addition of either 1 nM $FXIa_{WT}$ or 2–5 nM $FXIa_{G193}$ mutant. Initial rates of *p*NA release were measured on a SpectraMax 190 microplate reader (Molecular Devices, Sunnyvale, CA) at 405 nm, and converted to micromolar substrate released per minute. The IC_{50} (concentration of *p*AB required for 50% inhibition) was determined by fitting results with the IC_{50} four-parameter logistic equation of Halfman (eq 2) (28),

$$y = \frac{a}{1+(x/\mathrm{IC}_{50})^5} \quad (2)$$

where y is the rate of *p*NA release in the presence of a given concentration of *p*AB designated by x, a is the maximum rate of *p*NA release in the absence of *p*AB, and s is the slope factor. Each point was weighted equally and data was fitted to eq 2 using the nonlinear regression analysis program GraFit from Erithacus Software. To obtain $K_{\mathrm{d(app)}}$ values for the interaction of *p*AB with FXIa, we used eq 3, as described by Cheng and Prusoff (29) and elaborated on by Craig (30),

$$K_{\mathrm{d}p\mathrm{AB}} = \frac{\mathrm{IC}_{50}}{1+([\mathrm{S}]/K_{\mathrm{m}})} \quad (3)$$

where [S] is the S-2288 concentration. The K_{m} values obtained for each protease for S-2288 hydrolysis were used to obtain $K_{\mathrm{d(app)}}$.

Carbamylation of FXIa Ile[16] by Reaction with NaNCO

Carbamylation experiments were performed as described by Camire (31). Each reaction contained 1 μM FXIa in 20 mM Hepes, 0.15 M NaCl, 0.1% PEG, 2 mM $CaCl_2$, pH 7.5 (HBSP). Each experiment was performed in the absence or presence of *p*AB (10 times the $K_{\mathrm{d}\,p\mathrm{AB}}$). Reactions were started by addition of 0.2 M NaNCO. The pH after the addition of NaNCO was 7.5. Every 30 min, 5 μL aliquots were removed into 145 μL of HBSP containing 500 μM S-2288. Residual FXIa activity was determined from rates of hydrolysis using a Beckman DU 800 spectrophotometer, and plotted as a percent of initial activity. The k_{obs} for carbamylation were determined using eq 1.

Kinetics of FIX Activation

Sialyl-^{3}H-factor IX (specific activity 2.1×10^8 cpm/mg) was prepared as described (32). Labeled protein was a single band of appropriate molecular mass on reducing and nonreducing SDS–PAGE, and has ~85% of the activity of unlabeled FIX as measured in an activated partial thromboplastin time assay (32). The rate of FIX activation by FXIa was measured by determining the amount of ^{3}H-labeled FIX activation peptide released over time. Each reaction was carried out at 37 °C in TBS containing 0.5 mg/mL BSA, 5 mM $CaCl_2$, and FIX (2.0 μg/mL to 25 μg /mL). Reactions were initiated by addition of 0.25–25 nM FXIa. Aliquots (100 μL) were removed at various times into 100 μL of cold stop buffer (TBS, 50 mM benzamidine, 50 mM EDTA, and 5 mg/mL BSA). Equal volumes (200 μL) of 6% trichloroacetic acid (TCA) were added, followed by centrifugation to precipitate protein. Aliquots (100 μL) of TCA supernatant, which contain ^{3}H-labeled free activation peptide, were added to Aquasol 2 (4 mL), and ^{3}H was measured on a Beckman LS 5000CE β-counter. In the absence of FXIa, counts in the TCA supernatant were ≤1% of total counts (background), while complete FIX activation results in ~40% of the total counts in supernatant. Background counts (~1% of total) were subtracted from results for each sample to determine the amount of activity released by FXIa. The amount of FIXa formed was obtained from the average for three experiments, and rates of activation were determined by least-squares fitting of the data points to a straight line. Rates of activation were then plotted against FIX concentration, and K_{m} and k_{cat} were obtained using the Enzyme Kinetics program from Erithacus Software.

Inhibition of FXIa by Antithrombin in the Presence of Heparin

Reactions were carried out in 25 mM Tris-HCl, 100 mM NaCl pH 7.4, plus 0.1% Tween-20 (TBS-T) at 37 °C. FXIa (6 nM) was incubated with antithrombin (30 nM to 0.9 μM) in the presence of 1 unit/mL heparin. At various times, 20 μL samples were removed into 80 μL of TBS-T containing 500 μM S-2288 and 5 μg/mL Polybrene (to dissociate FXIa and heparin) in 96-well microtiter plates. Changes in absorbance at 405 nm were measured on a microplate reader, and residual FXIa activity was determined for each time point. Residual activity was plotted as a percent of initial activity, and the first-order rate constants (k_{obs}) were obtained for each concentration of antithrombin using eq 1, where A_t *and* A_0 are percent FXIa activity at time t and 0 s, respectively. The values of k_{obs} were plotted against the antithrombin concentration to obtain second-order rate constants.

Inhibition of FXIa with APPI

All reactions were carried out in TBS with 0.1 mg/mL BSA and 5 mM $CaCl_2$. Wild type FXIa or $FXIa_{G193A}$ (1 nM) or other FXIa mutants (10 nM) were incubated with various concentrations of APPI (10^{-1} to 10^5 nM) for 1 h at room temperature in a 96-well microtitration plate (total volume 100 μL). S-2288 (5 μL) was then added to a final concentration of 1 mM, and residual amidolytic activity was measured in a Molecular Devices V_{max} kinetic microplate reader. The apparent inhibition constant, K_i', was determined using the nonlinear regression data analysis program GraFit. Data for wild type FXIa and the $FXIa_{G193A}$ were analyzed with an equation for a tight-binding inhibitor (eq 4) where v_i and v_0 are the inhibited and uninhibited rates, respectively, and $[I]_0$ and $[E]_0$ are the total concentrations of inhibitor and enzyme, respectively (33,34).

$$v_i = v_0 \frac{\left(\left(K_i' + [I]_0 + [E]_0\right)^2 - 4[I]_0[E]_0\right)^{1/2} - \left(K_i' + [I]_0 - [E]_0\right)}{2[E]_0} \quad (4)$$

Inhibition data for $FXIa_{G193V}$, $FXIa_{G193E}$, $FXIa_{G193D}$, or $FXIa_{G193K}$, where K_i $[E]_0$, were analyzed using eq 5.

$$v_i = v_0 / \left(1 + [I]_0 / K_i'\right) \quad (5)$$

K_i values were obtained by correcting for the effect of substrate according to Beith et al. (33), using eq 6, where [S] is S-2288 concentration and K_m values were those for S-2288 hydrolysis (see above).

$$K_i = K_i' / (1 + (S) / K_m) \quad (6)$$

Molecular Modeling

The X-ray crystal structures of zymogen FXI (pdb code 2F83 (35)), FXIa with benzamidine (pdb code 1ZHM (36)), FXIa in complex with ecotin mutants containing amino acid replacements to mirror the activation peptide region of FIX (pdb codes 1XXF, 1XXD, and 1XX9 (37)), and FXIa in complex with APPI (pdb code 1ZJD (38)) were used for modeling. In each structure, Gly^{193} was changed to Ala, Asp, Glu, Lys, or Val and the local areas were energy minimized with slight adjustments. In modeling the 193 mutants, all residues could be fitted into the pocket occupied by Gly^{193}, and all bad contacts were relieved by minor

adjustments. The FXIa–ecotin structure containing the amino acid sequence surrounding the 180–181 FIX activation peptide region (pdb code 1XX9 (37)) was used to model the effect of Gly^{193} substitution on FIX binding, and the FXIa:APPI structure was used to model interactions and effects of the Gly^{193} substitutions on APPI binding (38). The trimolecular complex of antithrombin:heparin:thrombin (pdb code 1TB6 (39)) was used to model the FXIa: antithrombin complex and effects of Gly^{193} substitutions on antithrombin binding. Thrombin and FXIa were aligned and minor adjustments were made to correctly position FXIa with antithrombin.

RESULTS

FXIa Amidolytic Activity toward Small Synthetic Substrates

Initially we examined FXIa Gly^{193} mutants for perturbation of the S1, S2, and S4 substrate binding subsites and the oxyanion binding site, using two tripeptide substrates differing at the S4 site. The chromogenic substrate S-2288 has an isoleucyl side chain at S4, while S-2366 contains a pyroglutamyl group. These data are presented in Table 1. The K_m for both substrates was most affected when residue 193 had side chains that branch at the β-carbon (Val and Asp) and with a negative charge (Glu). It should be noted that the K_m and k_{cat} values for $FXIa_{G193V}$ and $FXIa_{G193D}$ for the substrate S-2366 are approximations because the value exceeded the highest substrate concentration used (10 mM). The k_{cat} values for both substrates were most affected by Val and Asp substitutions. The overall catalytic specificity constant (k_{cat}/K_m) was also most affected (~200-fold) with these two amino acid substitutions.

Inhibition of FXIa by DFP

The impairment in k_{cat} noted for S-2288 and S-2366 hydrolysis could in part stem from the inability of the mutants to stabilize the tetrahedral intermediate containing the oxyanion formed during catalysis (8,9). DFP specifically reacts with the active site serine (Ser^{195}) in these proteases and contains an oxyanion, making it a useful probe to test the integrity of the oxyanion hole (8,9,40,41). Results for DFP inhibition of $FXIa_{WT}$ and FXIa 193 mutants are shown in Figure 1 and summarized in Table 2. The oxyanion binding site is most impaired in $FXIa_{G193V}$ and $FXIa_{G193D}$, and the DFP binding data are consistent with the k_{cat} values for synthetic substrate hydrolysis by the $FXIa_{G193V}$ and $FXIa_{G193D}$.

Binding of pAB to FXIa

The K_m values for synthetic substrate hydrolysis reflect perturbation in the S1, S2, and/or S4 subsites. To ascertain the contributions of the S1 site toward impairment of synthetic substrate binding, we investigated the binding of *p*AB, which specifically interacts with Asp^{189}, located at the bottom of the S1 site. These data are presented in Figure 2 and summarized in Table 2. *p*AB binding was most impaired for $FXIa_{G193V}$ (36-fold) and $FXIa_{G193D}$ (14-fold), reflecting the increase in K_m values for synthetic substrate hydrolysis by these mutants.

Carbamylation of Ile^{16} Using NaNCO

Data in the previous sections indicate that the oxyanion hole and S1 site are not properly formed in FXIa with a non-Gly residue at position 193. Development of the S1 site and oxyanion hole in serine proteases requires formation of a salt bridge between the amino group of Ile^{16} and the carboxylate group of Asp^{194}. Covalent modification of the amino group of Ile^{16} by carbamylation results in an inactive enzyme, and a faster rate of carbamylation is indicative of a destabilized salt bridge. As summarized in Table 3, the rates of carbamylation for $FXIa_{G193D}$, $FXIa_{G193E}$ and $FXIa_{G193V}$ were 2.5–4-fold faster than for $FXIa_{WT}$. The rates of carbamylation of $FXIa_{G193A}$ and $FXIa_{G193K}$ were less impaired. Interestingly, these are the two amino acids that we have tested that do not have branched side chains. Occupancy of the

S1 site by *p*AB fully corrects the impairment (Table 3), consistent with earlier observations that occupancy of the S1 site stabilizes the Ile^{16}–Asp^{194} salt bridge in mutants of factor Xa and factor IXa (31,42).

FIX Activation by FXIa

FIX activation to the active proteases FIXaβ involves cleavage after Arg^{145} and Arg^{180} to liberate an 11 kDa activation peptide (43). FIX activation by FXIa was examined using an assay that measures liberation of the FIX activation peptide (32). These data are presented in Figure 3 and summarized in Table 4. The values for K_m were relatively similar for all proteases (167–268 nM), consistent with observations that exosite interactions distant from the protease active site are important in initial recognition and binding of FIX to FXIa (44-46). However, k_{cat} was decreased ~8-fold for $FXIa_{G193A}$ and ~400–1100-fold for the other mutants. The values for k_{cat} are influenced by the interaction of FXIa with both FIX activation cleavage sites and by catalysis of the FIX peptide bonds by FXIa. Therefore, values for k_{cat} represent cumulative effects of restricted binding and catalysis at the two activation sites.

FXIa Inhibition by Antithrombin and APPI

Antithrombin and APPI are physiologic inhibitors of FXIa. Antithrombin belongs to the serpin family of inhibitors, and its inhibition of FXIa is potentiated by heparin (47,48). The first-order rate constants, k_{obs}, for binding of antithrombin to $FXIa_{WT}$ and to FXIa mutants were plotted against antithrombin concentration (Figure 4). These data were used to obtain second-order rate constants (k_2), which are summarized in Table 5. The k_2 value for $FXIa_{G193A}$ inhibition was ~13-fold lower than for $FXIa_{WT}$, and ~1400–2300-fold lower for the other mutants. APPI, the protease inhibitory domain of the β-amyloid precursor protein, is a member of the Kunitz family of inhibitors (38,49). The overall binding constant (K_i) for inhibition by APPI was 22-fold greater for $FXIa_{G193A}$ and ~6500–27,000-fold greater for the other mutants (Figure 5, and summarized in Table 5).

DISCUSSION

Gly^{193} has two functional roles in an active serine protease: (1) it is part of the type II β-turn which allows the amide nitrogen to participate in formation of the oxyanion binding site, and (2) it allows the S2′ site to remain open for occupancy by the P2′ residue of substrates/inhibitors. In contrast, in protease zymogens, Gly^{193} is not part of a type II β-turn and the S2′ site is not formed. Therefore, replacing Gly^{193} with another residue is unlikely to have a significant effect on zymogen structure, as was observed in modeling studies (data not shown) with Ala, Asp, Glu, Lys, and Val at position 193 using the zymogen structure of FXI (34). This was also the case when zymogen FIX was modeled with Val at position 193 (20). Consistent with this premise, all recombinant FXI proteins used in the current study interacted similarly with the antibody used for affinity purification, which binds to the FXI protease domain, and all were activated similarly by FXIIa (data not shown). Substitution of Gly^{193} with a non-Gly residue in FXIa, on the other hand, is predicted to reorient the peptide bond between amino acids 192 and 193, causing the amide nitrogen of residue 193 to point away from the oxyanion binding site. Furthermore, it is anticipated that the size and nature of the residue 193 side chain will cause varying degrees of impairment by occupying the S2′ site. To test these concepts, we replaced Gly^{193} in FXIa with several naturally occurring substitutions observed in the blood coagulation serine proteases FVIIa and FIXa and compared them to the previously described $FXIa_{G193E}$ mutant (50).

The studies with small tripeptide substrates (S-2288 and S-2366) and inhibitors (DFP and *p*AB) demonstrate that interactions with the S1 sites and the oxyanion binding sites are most impaired in $FXIa_{G193D}$ and $FXIa_{G193V}$, to a lesser extent in $FXIa_{G193E}$ and $FXIa_{G193K}$, and

least impaired in $FXIa_{G193A}$ (Table 2). In general, these data agree with the impairment in formation of the salt bridge between Ile^{16} and Asp^{194}. The side chain of Val branches at the β-carbon, and Asp has a bulky carboxylate group at the β-carbon. These side chains are likely to perturb the local environment to a greater extent than the short side chain of Ala, or the unbranched side chain of Lys, which points into the solvent. In modeling studies the side chains with branching at the β-carbons impinge on the protease 140-loop (chymotrypsin numbering) and could cause distortion of the local region including the S1 site, the oxyanion binding site, the S2′ site, and possibly other interaction sites. It is interesting to note that, in the absence of S1 site occupancy, residues 189 through 194 are somewhat disordered in the structure of mouse glandular kallikrein-13 (11), one of the few serine proteases with a non-Gly residue 193 (Asp). These structural data are consistent with the deleterious effect of Asp or Val on both the S1 site and oxyanion binding sites in FXIa. The K_m for tripeptide substrates was most affected in $FXIa_{G193V}$ and $FXIa_{G193D}$, and least affected for $FXIa_{G193A}$ and $FXIa_{G193K}$ (Table 1), suggesting that S1 site occupancy contributes significantly toward impairment in the K_m. In interpreting these data, it must be recognized that the FXIa residue 193 side chains may adopt unanticipated conformations and/or interactions due to specific properties of the side chains and the local environment that are not accounted for in our analysis. Indeed, Asp^{193} in mouse glandular kallikrein-13 is part of a type II turn, in spite of the non-Gly residue at position 193, due to a unique salt bridge with Lys^{150} (11). Such interactions not only could influence formation of the oxyanion binding site, S1 site, and Ile^{16}–Asp^{194} salt bridge but also may affect accessibility of substrates and inhibitors to the active site.

Consistent with results for S-2288 and S-2366 cleavage, the k_{cat} for FIX activation was also most affected for $FXIa_{G193V}$ and $FXIa_{G193D}$ and least affected for $FXIa_{G193A}$ (Figure 3 and Table 3). However, the effects of mutations on k_{cat} for activation of FIX were significantly greater than for tripeptide substrates. With the exception of $FXIa_{G193A}$, where k_{cat} was impaired a modest 4.7-fold more for factor IX than for S-2288, k_{cat} for factor IX cleavage by the other mutants was impaired ~30–300-fold more than for the tripeptide substrates. Furthermore, again with the exception of $FXIa_{G193A}$, the k_{cat} for FIX cleavage did not vary as widely between mutants as did k_{cat} for tripeptide substrate hydrolysis. These results are consistent with modeling (Figure 6A), which indicates that the side chains of Asp, Glu, Lys, and Val all cause severe steric conflicts with the FIX P2′ residues Glu^{147} and Val^{182}. In the case of Lys or Glu, the long side chain causes significantly greater steric interference with the P2′ residue than do the side chains of Asp and Val, accounting for the relatively greater effect of Lys and Glu on FIX activation, relative to cleavage of tripeptide substrates or interactions with DFP or *p*AB.

Inhibition of $FXIa_{G193D}$, $FXIa_{G193V}$, $FXIa_{G193E}$ and $FXIa_{G193K}$ by antithrombin was impaired ~2000-fold, whereas inhibition of $FXIa_{G193A}$ was impaired only ~10-fold. The degree of impairment is somewhat greater than that seen for factor IX activation by these respective mutants. The P2′ residue in antithrombin is Leu, which is spatially somewhat larger than either Glu or the Val, the P2′ residues at the two activation cleavage sites in FIX. Thus, the P2′ Leu of antithrombin is expected to involve a larger area of the S2′ site and have steric conflicts with all the FXIa mutants with the exception of $FXIa_{G193A}$ (Figure 6B). This provides a rational explanation for the observed differences in impairment in FIX activation and antithrombin inhibition for various mutants. APPI has Met at the P2′ residue, the side chain of which is longer than the Leu in antithrombin. Thus, one would expect that the degree of impairment in the interaction between the FXIa mutants and APPI would be greater than was observed either for FIX or antithrombin. Indeed, such is the case in both the experimental and modeling (Figure 6C) studies.

The impairment in K_m and k_{cat} values in the FXIa mutants is consistent with our previous work with $FXIa_{G193E}$ (50) and with subsequent studies from other investigators (51,52). As K_m reflects ground state binding of substrate and k_{cat} reflects transition state binding, it appears

that both native and transition states of the enzyme are affected by a non-Gly residue at position 193. This conclusion is supported by evidence for impairment of both the oxyanion binding site (Figure 1) and the S1 binding site (Figure 2). A substitution for Gly^{193} likely affects the environment in the vicinity of the 192–193 peptide bond, as suggested by the structure of mouse glandular kallikrein-13 with Asp at position 193 (11).

Based on previous observations with FVIIa, occupancy of the S1 site by *p*AB, which does not contain an oxyanion group, likely does not restore the integrity of the oxyanion hole in non-Gly mutants (53). Furthermore, the energy required to restore the oxyanion binding site also likely depends on the nature of the 193 residue, with Ala having the least effect and Val and Asp (present study), and Pro (52) having the greatest effects. This may reflect the energy required to break interactions between the larger side chains of Asp, Val, Glu, and Lys and surrounding residues to allow rotation of the 192–193 bond so that the amide nitrogen of residue 193 points toward the oxyanion hole. In the case of Pro^{193}, the residue lacks an amide nitrogen preventing its participation in hydrogen bonding with the oxyanion of the substrate/inhibitor (52). The effects of residue 193 side chains on FXIa activity should apply to proteases such as FVIIa and FIXa, which have similar hydrophobic S2′ sites (36-38,53,54). Side chain branching at the β-carbon of residue 193 would be anticipated to be most detrimental in these proteases.

The side chain of residue 193 also contributes to specificity toward macromolecular substrates and inhibitors, depending on the P2′ residue of the substrate/inhibitor, as has been observed for human brain trypsin with Arg at position 193 (pdb code 1h4w (55)) and *Trimeresurus stejnejeri* plasminogen activator with Phe at position 193 (pdb code 1bqy (56)). The results for FXIa support this concept in that different amino acids at position 193 differentially affect interactions depending on whether Glu or Val (FIX), Leu (antithrombin), or Met (APPI) is the P2′ residue. In general, a serine protease with a non-Gly residue at position 193 would likely be restricted to cleaving substrates possessing Gly or short side chains residues at the P2′ position.

Acknowledgments

The authors thank Dr. Alvin Schmaier for providing the APPI protein used in these studies.

REFERENCES

1. Neaurath H, Walsh KA. Role of proteolytic enzymes in biological regulation (a review). Proc. Natl. Acad. Sci. U.S.A 1976;73:3825–3832. [PubMed: 1069267]
2. Davie EW, Fujikawa K, Kisiel W. The coagulation cascade: initiation, maintenance, and regulation. Biochemistry 1991;30:10363–10370. [PubMed: 1931959]
3. Sim RB, Tsiftsoglou SA. Proteases of the complement system. Biochem. Soc. Trans 2004;32:21–27. [PubMed: 14748705]
4. Busuttil SJ, Ploplis VA, Castellino FJ, Tang L, Eaton JW, Plow EF. A central role for plasminogen in the inflammatory response to biomaterials. J. Thromb. Haemostasis 2004;10:1798–1805. [PubMed: 15456492]
5. Daci E, Everts V, Torrekens S, Herck E, Tigchelaar-Gutterr W, Bouillon R, Carmeliet G. Increased bone formation in mice lacking plasminogen activators. J. Bone Miner. Res 2003;18:1167–1176. Van 1176. [PubMed: 12854826]
6. Bayer CA, Halsell SR, Fristrom JW, Kiehart DP, von Kalm L. Genetic interactions between the RhoA and Stubble-stubbloid loci suggest a role for a type II transmembrane serine protease in intracellular signaling during Drosophila imaginal disc morphogenesis. Genetics 2003;165:1417–1432. [PubMed: 14668391]
7. Honda A, Siruntawineti J, Baba T. Role of acrosomal matrix proteases in sperm-zona pellucida interactions. Hum. Reprod. Update 2002;5:405–412. [PubMed: 12398221]
8. Blow D. Enzymology. More of the catalytic triad. Nature 1990;343:694–695. [PubMed: 2304545]

9. Perona JJ, Craik CS. Structural basis of substrate specificity in the serine proteases. Protein Sci 1995;4:337–360. [PubMed: 7795518]
10. Schechter I, Berger A. On the size of the active site in proteases. I. Papain. Biochem. Biophys. Res. Commun 1967;27:157–162. [PubMed: 6035483]
11. Timm DE. The crystal structure of the mouse glandular kallikrein-13 (prorenin converting enzyme). Protein Sci 1997;6:1418–1425. [PubMed: 9232643]
12. Parry M, Jacob U, Huber R, Wisner A, Bon C, Bode W. The crystal structure of the novel snake venom plasminogen activator TSV-PA: a prototype structure for snake venom serine proteinases. Structure 1998;6:1195–1206. [PubMed: 9753698]
13. Katona G, Berglund G, Hajdu J, Graf L, Szilagyi L. Crystal structure reveals basis for the inhibitor resistance of human brain trypsin. J. Mol. Biol 2002;315:1209–1218. [PubMed: 11827488]
14. van Holde, KE.; Johnson, WC.; Ho, PS. Principles of Physical Biochemistry. Prentice Hall; Upper Saddle River, NJ: 1998. p. 42-44.
15. Zivelin A, Ogawa T, Bulvik S, Landau M, Toomey J, Lane J, Seligsohn U, Gailani D. Severe factor XI deficiency caused by a Gly555 to Glu mutation (factor XI-Glu555): a cross-reactive material positive variant defective in factor IX activation. J. Thromb. Haemostasis 2004;2:1782–1789. [PubMed: 15456490]
16. Thompson AR, Schoof JM, Weinmann AF, Chen S-H. Factor IX mutations: rapid, direct screening methods for 20 new families with hemophilia B. Thromb. Res 1992;65:289–295. [PubMed: 1579901]
17. Giannelli F, Green PM, Sommer SS, Lillicrap DP, Ludwig M, Schwaab R, Reitsma PH, Goossens M, Yoshioka A, Brownlee GG. Haemophilia B: database of point mutations and short additions and deletions. Nucleic Acids Res 1994;22:3534–3546. [PubMed: 7937052]
18. Saad S, Rowley G, Tagliavacca L, Green PM, Giannelli F, UK Haemophilia Centres. First report on UK database of haemophilia B mutations and pedigrees. Thromb. Haemostasis 1994;71:563–570. [PubMed: 8091381]
19. Van de Water NS, Williams R, Berry EW, Ockelford PA, Browett PJ. Factor IX gene mutations in haemophilia B: A New Zealand population based study. Haemophilia 1996;2:24–27.
20. Bajaj SP, Spitzer SG, Welsh WJ, Warn-Cramer BJ, Kasper CK, Birktoft JJ. Experimental and theoretical evidence supporting the role of Gly363 in blood coagulation factor IXa (Gly193 in chymotrypsin) for proper activation of the proenzyme. J. Biol. Chem 1990;265:2956–2961. [PubMed: 2303434]
21. Bernardi F, Liney DL, Patracchini P, Gemmati D, Legnani C, Arcieri P, Pinotti M, Redaelli R, Ballerini G, Pemberton S, Wacey AI, Mariani G, Tuddenham EGD, Marchetti G. Molecular defects in CRM+ factor VII deficiencies: modeling of missense mutations in the catalytic domain of FVII. Br. J. Haematol 1994;86:610–618. [PubMed: 8043443]
22. Bernardi F, Castaman G, Pinotti M, Ferraresi P, Di Iasio MG, Lunghi B, Rodeghiero, Marchetti GF. Mutation pattern in clinically asymptomatic coagulation factor VII deficiency. Hum. Mutat 1996;8:108–115. [PubMed: 8844208]
23. Bouma BN, Griffin JH. Human blood coagulation factor XI. Purification, properties, and mechanism of activation by activated factor XII. J. Biol. Chem 1977;252:6432–6437. [PubMed: 893417]
24. Butenas S, Mann KG. Blood coagulation. Biochemistry (Moscow) 2002;67:3–12. [PubMed: 11841335]
25. Fujikawa K, Chung DW, Hendrickson LE, Davie EW. Amino acid sequence of human factor XI, a blood coagulation factor with four tandem repeats that are highly homologous with plasma prekallikrein. Biochemistry 1986;25:2417–2424. [PubMed: 3636155]
26. Sun MF, Zhao M, Gailani D. Identification of amino acids in the factor XI apple 3 domain required for activation of factor IX. J. Biol. Chem 1999;274:36373–36378. [PubMed: 10593931]
27. Lottenberg R, Jackson CM. Solution composition dependent variation in extinction coefficients for p-nitroaniline. Biochem. Biophys. Acta 1983;742:558–564. [PubMed: 6838889]
28. Halfman CJ. Concentrations of binding protein and labeled analyte that are appropriate for measuring at any analyte concentration range in radioimmunoassays. Methods Enzymol 1981;74:481–497. [PubMed: 7321893]

29. Cheng Y-C, Prusoff WH. Relationship between the inhibition constant (K1) and the concentration of inhibitor which causes 50 per cent inhibition (I50) of an enzymatic reaction. Biochem. Pharmacol 1973;22:3099–3108. [PubMed: 4202581]
30. Craig DA. The Cheng-Prusoff relationship: something lost in the translation. Trends Pharmacol. Sci 1993;14:89–91. [PubMed: 8488569]
31. Camire RM. Prothrombinase assembly and S1 site occupation restore the catalytic activity of FXa impaired by mutation at the sodium-binding site. J. Biol. Chem 2002;277:37863–37870. [PubMed: 12149252]
32. Bajaj SP, Birktoft JJ. Human factor IX and factor IXa. Methods Enzymol 1993;222:96–128. [PubMed: 8412817]
33. Beith JG. In vivo significance of kinetic constants of protein proteinase inhibitors. Biochem. Med 1984;32:287–397.
34. Morrison JF, Walsh CT. The behavior and significance of slow-binding enzyme inhibitors. Adv. Enzymol. Relat. Areas Mol. Biol 1988;61:201–301. [PubMed: 3281418]
35. Papagrigoriou E, McEwan PA, Walsh PN, Emsley J. Crystal structure of the factor XI zymogen reveals a pathway for transactivation. Nat. Struct. Mol. Biol 2006;13:557–558. [PubMed: 16699514]
36. Jin L, Pandey P, Babine RE, Weaver DT, Abdel-Meguid SS, Strickler JE. Mutation of surface residues to promote crystallization of activated factor XI as a complex with benzamidine: an essential step for the iterative structure-based design of factor XI inhibitors. Acta Crystallogr., Sect. D: Biol. Crystallogr 2005;61:1418–1425. [PubMed: 16204896]
37. Jin L, Pandey P, Babine RE, Gorga JC, Seidl KJ, Gelfand E, Weaver DT, Abdel-Meguid SS, Strickler JE. Crystal structures of the FXIa catalytic domain in complex with ecotin mutants reveal substrate-like interactions. J. Biol. Chem 2005;280:4704–4712. [PubMed: 15545266]
38. Navaneetham D, Jin L, Pandey P, Strickler JE, Babine RE, Abdel-Meguid SS, Walsh PN. Structural and mutational analyses of the molecular interactions between the catalytic domain of factor XIa and the Kunitz protease inhibitor domain of protease nexin 2. J. Biol. Chem 2005;280:36165–36175. [PubMed: 16085935]
39. Li W, Johnson DJ, Esmon CT, Huntington JA. Structure of the antithrombin-thrombin-heparin ternary complex reveals the antithrombotic mechanism of heparin. Nat. Struct. Mol. Biol 2004;11:857–862. [PubMed: 15311269]
40. Huber R, Bode W. Structural basis of the activation and action of trypsin. Acc. Chem. Res 1978;11:114–122.
41. Kraut J. Serine proteases: Structure and mechanism of catalysis. Ann. Rev. Biochem 1977;46:331–358. [PubMed: 332063]
42. Schmidt AE, Stewart JE, Mathur A, Krishnaswamy S, Bajaj SP. Na+ site in blood coagulation factor IXa: effect on catalysis and factor VIIIa binding. J. Mol. Biol 2005;350:78–91. [PubMed: 15913649]
43. DiScipio R, Kurachi K, Davie E. Activation of human factor IX (Christmas Factor). J. Clin. Invest 1978;61:1528–1538. [PubMed: 659613]
44. Ogawa T, Verhamme IM, Sun MF, Bock PE, Gailani D. Exosite-mediated substrate recognition of factor IX by factor XIa. The factor XIa heavy chain is required for initial recognition of factor IX. J. Biol. Chem 2005;280:23523–23530. [PubMed: 15829482]
45. Aktimur A, Gabriel MA, Gailani D, Toomey JR. The factor IX gamma-carboxyglutamic acid (Gla) domain is involved in interactions between factor IX and factor XIa. J. Biol. Chem 2003;278:7981–7987. [PubMed: 12496253]
46. Baglia FA, Jameson BA, Walsh PN. Identification and chemical synthesis of a substrate-binding site for factor IX on coagulation factor XIa. J. Biol. Chem 1991;266:24190–24197. [PubMed: 1748688]
47. Soons H, Janssen-Claesson T, Tans G, Hemker H. Inhibition of factor XIa by antithrombin III. Biochemistry 1989;26:4624–4629. [PubMed: 3499176]
48. Beeler D, Marcum J, Schiffman S, Rosenberg R. Interaction of factor XIa and antithrombin in the presence and absence of heparin. Blood 1986;67:1488–1492. [PubMed: 3486013]
49. Schmaier AH, Dahl LD, Rozemuller AJ, Roos RA, Wagner SL, Chung R, Van Nostrand WE. Protease nexin-2/amyloid beta protein precursor. A tight-binding inhibitor of coagulation factor IXa. J. Clin. Invest 1993;92:2540–2545. [PubMed: 8227367]

50. Schmidt A, Ogawa T, Gailani D, Bajaj SP. Structural role of Gly(193) in serine proteases: investigations of a G555E (Gly193 in chymotrypsin) mutant of blood coagulation factor XI. J. Biol. Chem 2004;279:29485–29492. [PubMed: 15090552]
51. Toth J, Gombos L, Simon Z, Medveczky P, Szilagyi L, Graf L, Malnasi-Csizmadia A. Thermodynamic analysis reveals structural rearrangement during the acylation step in human trypsin 4 on 4-methylumbelliferyl 4-guanidinobenzoate substrate analogue. J. Biol. Chem 2006;281:12596–12602. [PubMed: 16492676]
52. Bobofchak KM, Pineda AO, Mathews FS, Di Cera E. Energetic and structural consequences of perturbing Gly-193 in the oxyanion hole of serine proteases. J. Biol. Chem 2005;280:25644–25650. [PubMed: 15890651]
53. Bajaj SP, Schmidt AE, Agah S, Bajaj MS, Padmanabhan K. High resolution structures of p-aminobenzamidine- and benzamidine-VIIa/soluble tissue factor: unpredicted conformation of the 192-193 peptide bond and mapping of Ca2+, Mg2+, Na+, and Zn2+ sites in factor VIIa. J. Biol. Chem 2006;281:24873–24888. [PubMed: 16757484]
54. Hopfner KP, Lang A, Karcher A, Sichler K, Kopetzki E, Brandstetter H, Huber R, Bode W, Engh RA. Coagulation factor IXa: the relaxed conformation of Tyr99 blocks substrate binding. Structure 1999;7:989–996. [PubMed: 10467148]
55. Katona G, Berglund GI, Hajdu J, Graf L, Szilagyi L. Crystal structure reveals basis for the inhibitor resistance of human brain trypsin. J. Mol. Biol 2002;315:1209–1218. [PubMed: 11827488]
56. Parry MAA, Jacob U, Huber R, Wisner A, Bon C, Bode W. The crystal structure of the novel snake venom plasminogen activator TSV-PA: a prototype structure for snake venom serine proteinases. Structure 1998;6:1195–1206. [PubMed: 9753698]
57. Jones TA, Zou JY, Cowan SW, Kjeldgaard M. Improved methods for building protein models in electron density maps and the location of errors in these models. Acta Crystallogr. A 1991;47:110–119. [PubMed: 2025413]

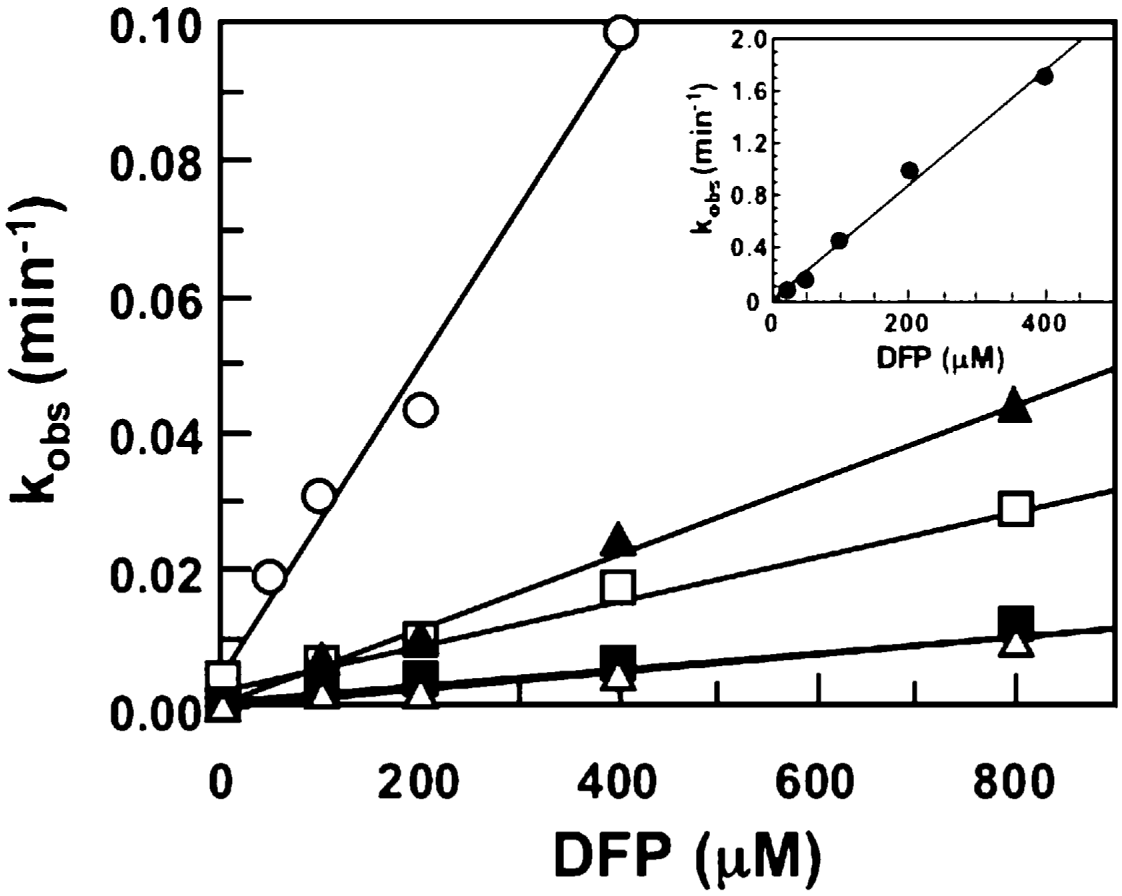

Figure 1.

Inhibition of FXIa by DFP. Each reaction was carried out in TBS/BSA, 5 mM $CaCl_2$ at room temperature. The concentration for FXIa was 250 nM, and DFP was added at various concentrations up to 800 μM. At various times, 5 μL aliquots were removed and added to 155 μL of TBS/BSA containing 625 μM S-2288. The percent residual FXIa activity at each point was plotted as a function of time to obtain the values of k_{obs}. The first-order rate constants, k_{obs}, are plotted against the DFP concentration. $FXIa_{G193A}$ (○), $FXIa_{G193D}$ (■), $FXIa_{G193E}$ (□), $FXIa_{G193K}$ (▲), and $FXIa_{G193V}$ (△). Inset: $FXIa_{WT}$ (●).

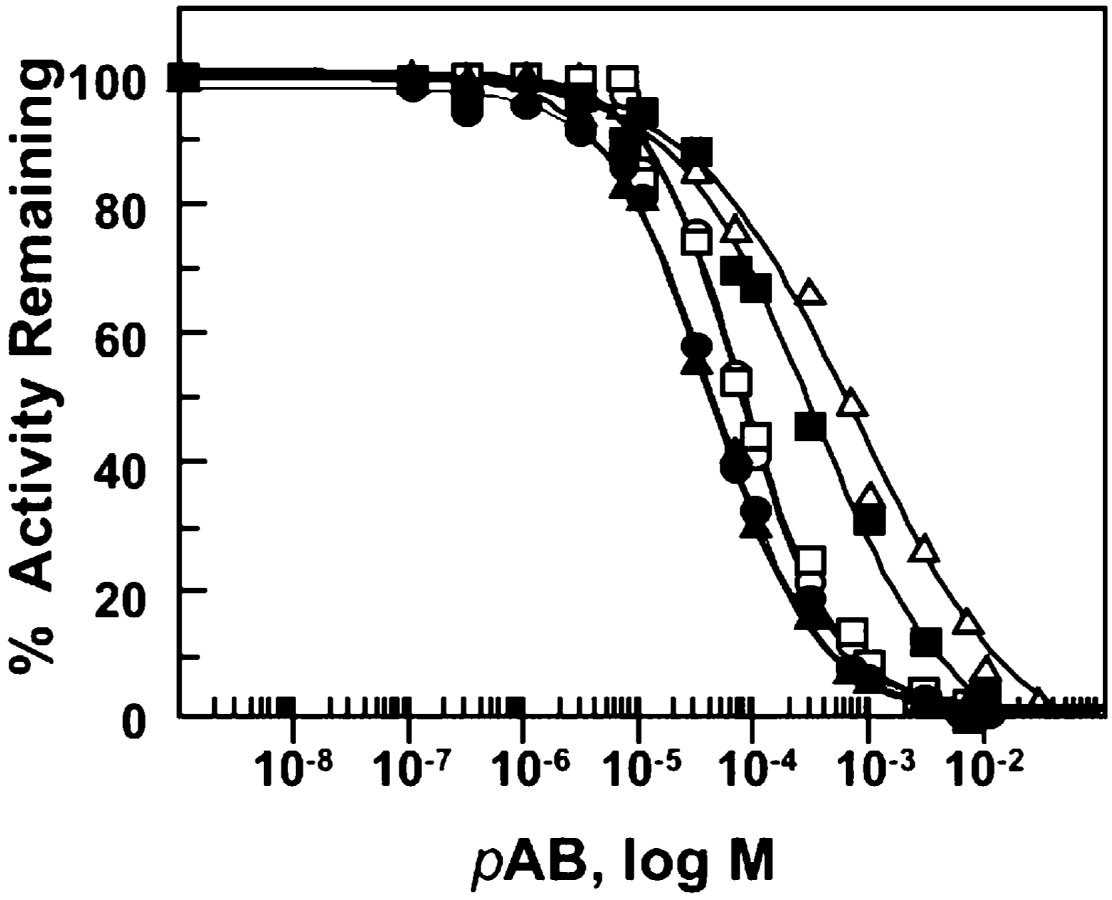

Figure 2.

Binding of *p*AB to FXIa. Each reaction was carried out in TBS with 5 mM Ca^{2+}, 100 μg/mL BSA, and either 100 μM S-2288 (for $FXIa_{WT}$) or 500 μM S-2288 (for $FXIa_{G193}$ mutants). Increasing amounts of *p*AB were added to each mixture, and the reactions were initiated by addition of either 1 nM $FXIa_{WT}$ or 2–5 nM $FXIa_{G193}$ mutant. Initial rates of *p*NA release were measured and converted to μM substrate hydrolyzed/min, and the percent activity was plotted as a function of *p*AB concentration. $FXIa_{WT}$ (●), $FXIa_{G193A}$ (○), $FXIa_{G193D}$ (■), $FXIa_{G193E}$ (□), $FXIa_{G193K}$ (▲), and $FXIa_{G193V}$ (△).

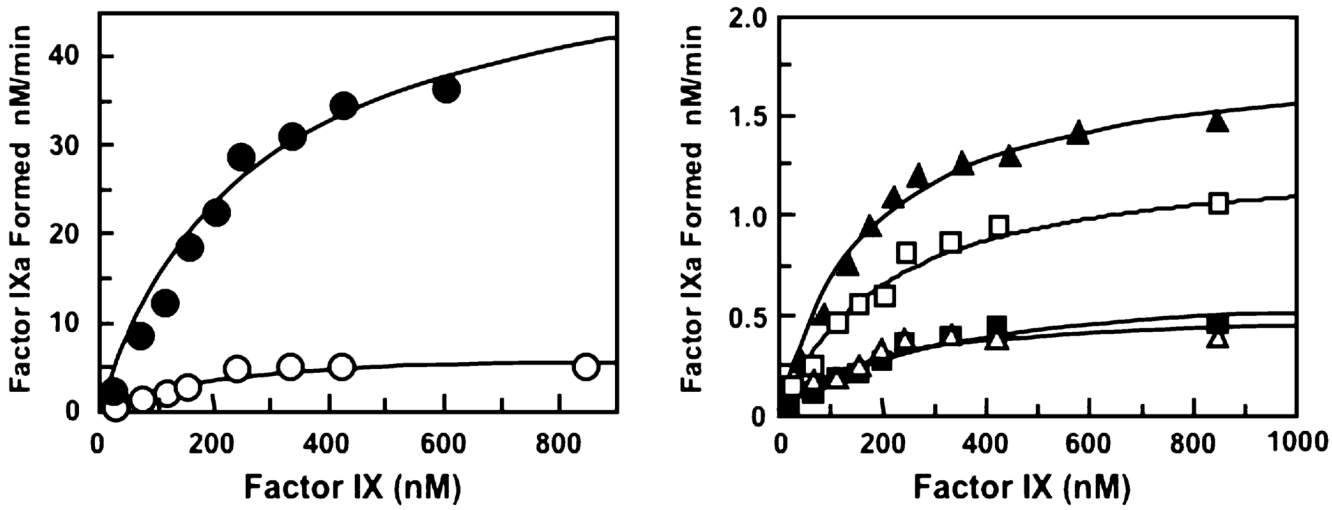

Figure 3.

FIX activation by FXIa. The rate of FIX activation was determined by measuring activation peptide released during incubation with FXIa. Reactions were carried out in TBS containing 0.5 mg/mL BSA and 5 mM $CaCl_2$ at 37 °C. The concentration of FIX varied from 25 to 850 μM, and the concentration of FXIa was 0.25–25 nM. The data are normalized to 25 nM FXIa. $FXIa_{WT}$ (●), $FXIa_{G193A}$ (○), $FXIa_{G193D}$ (■), $FXIa_{G193E}$ (□), $FXIa_{G193K}$ (▲), and $FXIa_{G193V}$ (△).

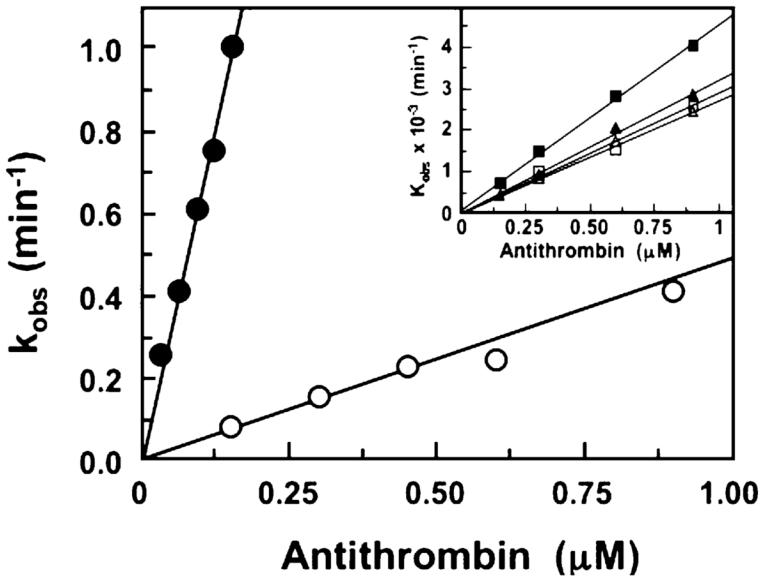

Figure 4.

Inhibition of FXIa by antithrombin. Reactions were carried out in TBS with 0.1% Tween-20 and 5 mM $CaCl_2$ at 37 °C containing FXIa (6–12 nM) and antithrombin (30 nM to 1.8 μM). At various times, residual FXIa activity was measured as described under Experimental Procedures to obtain the first-order rate constants, k_{obs}. k_{obs} is shown plotted against antithrombin concentration. Main panel: $FXIa_{WT}$ (●) and $FXIa_{G193A}$ (○). Inset: $FXIa_{G193D}$ (■), $FXIa_{G193E}$ (□), $FXIa_{G193K}$ (▲), and $FXIa_{G193V}$ (△).

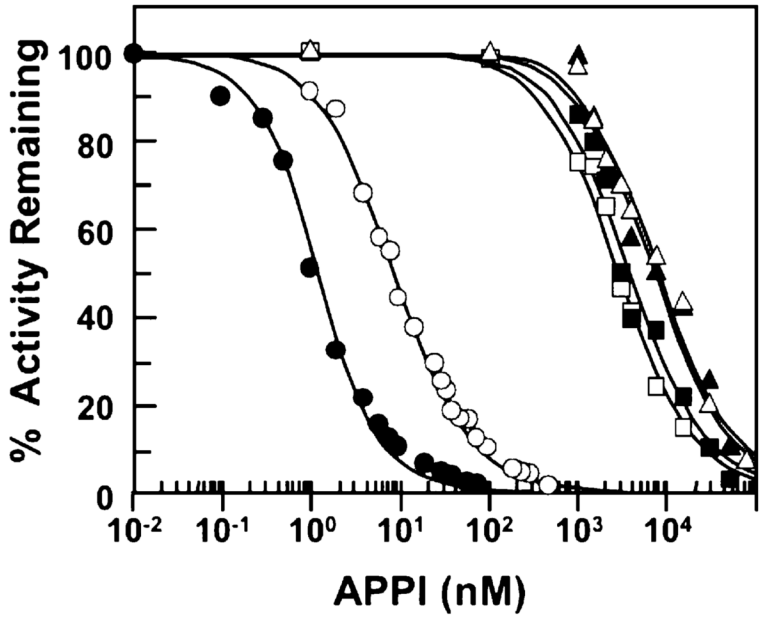

Figure 5.

Inhibition of FXIa by APPI. Reactions were carried out in TBS with 0.1 mg/mL BSA and 5 mM $CaCl_2$ at room temperature. Wild type FXIa or the Ala mutant (1 nM each), or other FXIa mutants (10 nM) were incubated with various concentrations of APPI for 1 h, followed by addition of S-2288 to a final concentration of 1 mM. Residual amidolytic activity was measured on a microtiter plate reader and plotted against inhibitor concentration. Results for wild type FXIa and the Ala mutant were analyzed with eq 4, and results for other mutants were analyzed with eq 5 (Experimental Procedures). $FXIa_{WT}$ (●), $FXIa_{G193A}$ (○), $FXIa_{G193D}$ (■), $FXIa_{G193E}$ (□), $FXIa_{G193K}$ (▲), and $FXIa_{G193V}$ (△).

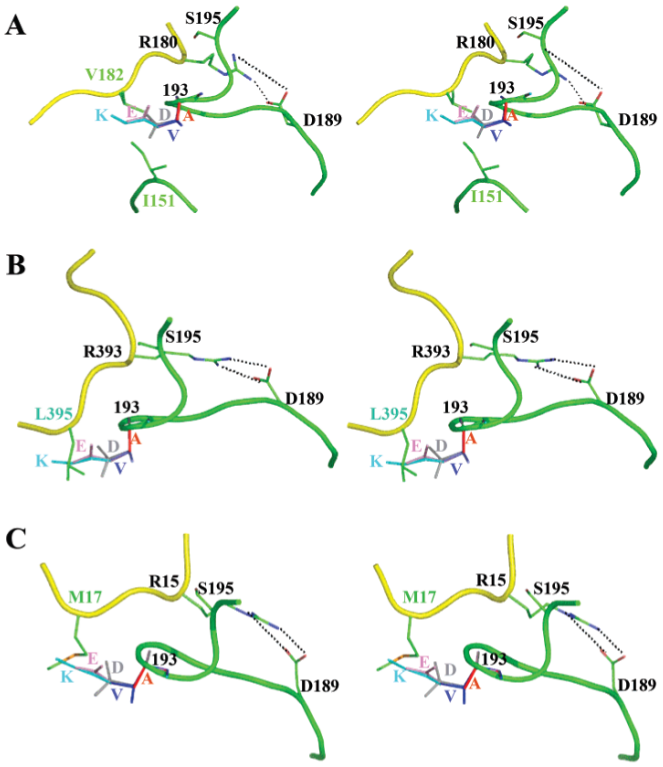

Figure 6.

Stereo images of the steric conflicts between residue 193 side chains of FXIa mutants and the P2′ residues of FIX, antithrombin, and APPI. For all images, FXIa is shown as a green ribbon and FIX, antithrombin or APPI are shown as yellow ribbons. The side chains of FXIa Asp^{189} and the P1 Arg and P2′ residues of FIX, antithrombin, and APPI are also shown in green. Oxygens on the side chain of FXIa Asp^{189} are in red, and nitrogens on the side chains of the P1 Arg residues are in blue. The side chain of Asp^{189} in FXIa forms bidentate salt bridges (dashed lines) with the P1 residues (FIX Arg^{180}, antithrombin Arg^{393}, APPI Arg^{15}). The positions of carbon atoms and carbon–carbon bonds in the side chains of FXIa 193 residues are shown in red for $FXIa_{G193A}$ (A), blue for $FXIa_{G193V}$ (V), gray for $FXIa_{G193D}$ (D), pink for $FXIa_{G193E}$ (E), and cyan for $FXIa_{G193K}$ (L). (A) FIX. The model is based on the structure of FXIa with ecotin containing the P5 to P2′ residues of the FIX activation cleavage site at the C-terminal of the activation peptide (39). Ile^{151} of FXIa is also shown. Note that the side chain of the FIX P2′ residue Val^{182} conflicts with larger side chains at FXIa 193. (B) Antithrombin. The structure of the antithrombin: thrombin complex (pdb code 1TB6 (39)) was used to model the FXIa:antithrombin complex. The graphics program package O (57) was used to replace the protease domain of thrombin with the protease domain of FXIa. Note that the side chain of the antithrombin P2′ residue Leu^{395} conflicts with larger side chains at FXIa 193. (C) APPI. FXIa residue 193 mutations were introduced into the structure of FXIa:APPI (37) using graphics program package O (57). Note that the side chain of the APPI P2′ residue Met^{17} conflicts with some of the larger side chains at FXIa 193.

Table 1

Kinetic Parameters for FXIa Hydrolysis of Synthetic Substrates[a]

	S-2288			S-2366		
protein	K_m **(mM)**	k_{cat} **(s^{-1})**	k_{cat}/K_m **(mM^{-1} s^{-1})**	K_m **(mM)**	k_{cat} **(s^{-1})**	k_{cat}/K_m **(mM^{-1} s^{-1})**
$FXIa_{WT}$	0.34 ± 0.02	110.2 ± 1.8	324 (1)[b]	0.26 ± 0.02	145 ± 1.8	559 (1)[b]
$FXIa_{G193A}$	1.39 ± 0.17	64.8 ± 5.3	47 (7)	1.19 ± 0.13	117.0 ± 9.0	98 (6)
$FXIa_{G193V}$	4.78 ± 0.82[c]	10.0 ± 1.0	2 (162)	13.64 ± 1.46[c]	26.7 ± 1.5	2 (280)
$FXIa_{G193D}$	2.70 ± 0.60	4.2 ± 0.5	1.6 (202)	13.93 ± 2.13[c]	40.8 ± 3.0	3 (186)
$FXIa_{G193E}$	2.91 ± 0.31	71.2 ± 3.4	25 (13)	2.35 ± 0.15	98.0 ± 2.9	42 (13)
$FXIa_{G193K}$	1.38 ± 0.22	30.0 ± 1.8	22 (15)	1.85 ± 0.19	114.2 ± 4.7	62 (9)

[a] Increasing amounts of S-2288 or S-2366 were added to reactions containing 1–5 nM FXIa in TBS, pH 7.5, 100 μg/mL BSA and 5 mM $CaCl_2$. The rates of *p*NA release were measured as described under Experimental Procedures. Data are averages for three separate experiments.

[b] The fold-change in specificity constant (in parentheses) represents a comparison to results for $FXIa_{WT}$.

[c] K_m is approximate because the highest concentration of substrate tested was near or below actual K_m.

Table 2

DFP Inhibition of FXIa and pAB Binding to FXIa[a]

protein	DFP		*p*AB	
	k_2 (M^{-1} min^{-1})	fold-decrease[b]	$K_{d\ pAB}$ (μM)	fold-change[b]
FXI_{aWT}	6110.4 ± 41	1.0	19.0 ± 1.0	1.0
$FXIa_{G193A}$	171.5 ± 26	35	55.6 ± 3.5	3.0
$FXIa_{G193V}$	11.5 ± 1.1	532	689.2 ± 59	36.3
$FXIa_{G193D}$	12.8 ± 1.2	478	269.7 ± 55	14.2
$FXIa_{G193E}$	32.3 ± 4.9	189	85.5 ± 8.9	4.5
$FXIa_{G193K}$	54.6 ± 7.8	112	30.1 ± 1.6	1.6

[a] Each reaction contained 250 nM FXIa in TBS/BSA, 5 mM $CaCl_2$ at room temperature. DFP (2 μM to 4 mM) was added, and the residual FXIa activity was plotted as a function of time to obtain the values for k_{obs} (first-order rate constants), as described in Experimental Procedures. Values for k_{obs} were plotted against DFP concentration (Figure 1) to determine the second-order rate constants shown in the table. Increasing amounts of *p*AB (10^{-2} to 10^{-7} M) were added to each reaction containing S-2288 and FXIa, and residual FXIa activity was determined by measuring *p*NA release (Figure 2). The apparent $K_{d\ pAB}$ values were calculated using eq 2 as described under Experimental Procedures. Results for both DFP and *p*AB are averages of three experiments.

[b] The fold-decrease for DFP and fold-change for *p*AB are in comparison to values for $FXIa_{WT}$.

Table 3

Kinetic Parameters for Carbamylation of Ile^{16} in FXIa[a]

protein	no *p*AB		saturating *p*AB	
	rate constant (M^{-1} min^{-1})	fold-change[b]	rate constant (M^{-1} min^{-1})	fold-change[c]
$FXIa_{WT}$	15.4 ± 0.9	1.0[b]	6.8 ± 0.5	1.0[b]
$FXIa_{G193A}$	35.4 ± 1.6	2.3	6.4 ± 0.8	0.9
$FXIa_{G193V}$	49.9 ± 1.7	3.2	6.3 ± 1.0	0.9
$FXIa_{G193D}$	38.5 ± 1.4	2.5	4.3 ± 0.6	0.6
$FXIa_{G193E}$	51.5 ± 1.3	4.0	7.9 ± 1.0	1.2
$FXIa_{G193K}$	20.8 ± 1.2	1.4	5.4 ± 0.3	0.8

[a] The rates of carbamylation of the free amino group of Ile16 of FXIa were measured over a period of 5 h as described under Experimental Procedures. Upon carbamylation, FXIa becomes inactive and cannot hydrolyze a synthetic substrate. Aliquots of each reaction, run either in the presence or in the absence of saturating amounts of *p*AB, were removed every 30 min and assayed for residual FXIa activity. Results are averages for two experiments.

[b] Fold-change is compared to the carbamylation rate for FXIaWT in the absence of *p*AB.

[c] Fold-change is compared to the carbamylation rate for FXIaWT in the presence of *p*AB.

Table 4

Kinetics of FIX Activation by FXIa[a]

protein	K_m (nM)	k_{cat} (min^{-1})	fold-change in k_{cat}[b]
$FXIa_{WT}$	268 ± 25	21.816 ± 2.160	1[b]
$FXIa_{G193A}$	226 ± 33	2.782 ± 0.052	8
$FXIa_{G193V}$	167 ± 17	0.021 ± 0.003	1091
$FXIa_{G193D}$	258 ± 28	0.026 ± 0.003	853
$FXIa_{G193E}$	236 ± 33	0.048 ± 0.005	455
$FXIa_{G193K}$	256 ± 31	0.055 ± 0.006	397

[a]The rate of FIX activation was determined by measuring the amount of radioactive peptide released at various times in incubations with FXIa, as described under Experimental Procedures. Each reaction was carried out in TBS containing 0.5 mg/mL BSA and 5 mM $CaCl_2$ at 37 °C, with concentrations of FIX varying from 25 to 775 nM, and FXIa concentrations varying from 0.25 to 25 nM. The data are normalized to 25 nM FXIa.

[b]Fold-change is compared to FIX activation by $FXIa_{WT}$.

Table 5

FXIa Inhibition by Antithrombin or APPI[a]

	antithrombin		APPI		
protein	***k*2 (mM^{-1} min^{-1})**	**fold-proteindecrease**	**apparent $K_i$protein(nM) (K_i')**	**K_i (nM)**	**fold-change**
$FXIa_{WT}$	6420 ± 250	1[b]	0.72 ± 0.02	0.061	1[b]
$FXIa_{G193A}$	486 ± 30	13	8.96 ± 0.21	6.58	22
$FXIa_{G193V}$	2.8 ± 0.2	2292	8652 ± 251	7865	27,027
$FXIa_{G193D}$	4.4 ± 1.1	1460	3913 ± 148	3288	13,446
$FXIa_{G193E}$	2.9 ± 0.1	2213	2975 ± 104	1891	6498
$FXIa_{G193K}$	3.2 ± 0.2	2006	7752 ± 321	5701	19,591

[a]Reactions containing FXIa (6-12 nM) and antithrombin (0.03-0.9 μM) were carried out in TBS, 0.1% Tween-20, 5 mM $CaCl_2$ at 37 °C. At various times, residual FXIa activity was measured as described in Experimental Procedures. Residual FXIa activity at each time point was plotted as a function of time to obtain the values for kobs (first-order rate constant). Values for kobs were plotted against antithrombin concentration to determine the second-order rate constant (k_2). APPI (10^{-1} to 10^5 nM) and FXIa (0.5–10 nM) were incubated for 1 h at room temperature in TBS, 100 μg/mL BSA, 5 mM $CaCl_2$. S-2288 was added to a final concentration of 1 nM, and pNA release was measured. The data were analyzed as described in Experimental Procedures.

[b]Fold-decrease is in comparison to the result for $FXIa_{WT}$.